Research Square

Preprints are preliminary reports that have not undergone peer review.
They should not be considered conclusive, used to inform clinical practice,
or referenced by the media as validated information.

Arrhenius-Based Capacity and Dispatch Optimization of a Wind–Photovoltaic–Storage Microgrid Using Task-Preserving, Degradation-Aware Refinement

Ranran Wang
Shandong Agricultural University
Jiayu Wang
Shandong Agricultural University
Xinyu Yu
Shandong Agricultural University
Zeyu Qiu
Shandong Agricultural University
Wenqiao Li
Shandong Agricultural University
Jiancheng Wang
wangjc@sdtaikai.com

Shandong Taikai High Voltage Switchgear Co., Ltd.

Research Article

Keywords: wind–photovoltaic–storage microgrid, capacity–dispatch co-optimization, Arrhenius battery degradation, feasibility repair, task-preserving trajectory refinement

Posted Date: November 13th, 2026

DOI: https://doi.org/10.21203/rs.3.rs-11539085/v1

License: This work is licensed under a Creative Commons Attribution 4.0 International License.
Read Full License

Additional Declarations: No competing interests reported.

Arrhenius-Based Capacity and Dispatch Optimization of a Wind–Photovoltaic–Storage Microgrid Using Task-Preserving, Degradation-Aware Refinement

Ranran Wang*, Jiayu Wang*, Xinyu Yu*, Zeyu Qiu*, Wenqiao Li*, Jiancheng Wang**‡

*College of Mechanical and Electronic Engineering, Shandong Agricultural University, Tai'an, Shandong 271018, China

**Shandong Taikai High Voltage Switchgear Co., Ltd., High-Tech Industrial Development Zone, Tai'an, Shandong 271000, China

wangranran@sdau.edu.cn, 734028686@qq.com, 13031769117@163.com, 3065344250@qq.com, 1274309976@qq.com

‡ Corresponding author: Jiancheng Wang. Email: wangjc@sdtaikai.com

Abstract

Feasibility repair can change the state-of-charge (SOC) trajectory used to evaluate battery degradation. We develop a cost–carbon–degradation model for a grid-connected wind–photovoltaic–storage microgrid. After correcting each schedule to meet a common daily terminal SOC, a degradation-aware refinement shifts charging and discharging between admissible hours while preserving their respective daily energy totals. An improved nondominated sorting genetic algorithm II (NSGA-II) combining differential evolution, adaptive variation and structured local search uses 24,000 objective evaluations in each of 12 independent runs. Across the 12 runs, the improved NSGA-II achieved a mean inverted generational distance (IGD) of 0.02840 ± 0.00168 and a normalized hypervolume (HV) of 0.84665 ± 0.00444. The corresponding mean values for standard NSGA-II were 0.08489 and 0.72758. The representative solution from the run closest to the median IGD is rated at 40.49 MW/114.97 MWh. Across 12 candidate pairs with matched ratings and daily charge and discharge totals, refinement reduces modeled first-year capacity loss by 10.70% ± 1.11% on average. Fixed-trajectory sensitivity across 17 degradation-model settings gives mean reductions in modeled first-year loss of 0.39% to 16.19%; two candidates instead show increased loss in the anchored linear case. These results show that the degradation benefit of temporal redistribution depends on the assumed aging model and that feasibility-repair choices can affect degradation assessment.

Keywords: wind–photovoltaic–storage microgrid; capacity–dispatch co-optimization; Arrhenius battery degradation; feasibility repair; task-preserving trajectory refinement

1 Introduction

Battery storage shifts renewable surplus to periods of demand, coupling installed capacity with hourly operation in grid-connected microgrids. Studies of zero-carbon microgrids and flexibility resources highlight this interaction (Chen et al., 2024; Gharibvand et al., 2024; Zhou, 2024). Capacity–dispatch coordination has been investigated through variability management, layered scheduling and multiobjective wind–solar–storage sizing (Wang et al., 2024; Xie et al., 2022; Zhao et al., 2024), while environmental accounting and multiscale operation introduce further trade-offs among cost, emissions and storage dispatch (Dong et al., 2023; Jiménez-Vargas et al., 2023). Battery energy capacity determines the available energy headroom and, together with the power rating, constrains charging and discharging rates; dispatch determines when the battery operates. Consequently, the value of a storage configuration depends on both its rating and the trajectory used to operate it.

This coupling also makes battery degradation relevant to both sizing and dispatch. Mehmood et al. (2017) and Cardoso et al. (2018) incorporated battery aging into planning, while Amini et al. (2021), Fallahifar and Kalantar (2023), and Amini et al. (2024) considered capacity deterioration, replacement or thermal effects. Temperature, state-of-charge (SOC) residence and cycling conditions produce different degradation responses (Gasper et al., 2023; Schmalstieg et al., 2014). Related models have been applied to microgrid management and hybrid-system design (Pinciroli et al., 2023; Safavi et al., 2025; Seger et al., 2023; Superchi et al., 2025), alongside economic and environmental optimization (Dai & Batool, 2024; Jin et al., 2024; Kassab et al., 2024). These studies motivate consideration of aging alongside capacity and operation, while the trajectory used to evaluate aging can itself depend on how operating constraints are enforced.

Recent studies have combined economic, environmental and battery-aging considerations in different ways. Li et al. (2025) incorporated storage degradation cost and carbon trading into multiobjective microgrid energy management and used TOPSIS to select an operating strategy. Altimania et al. (2026) combined operating cost, battery degradation and grid-related emissions in a weighted energy-management formulation. For capacity planning, Agha Kassab et al. (2025) jointly considered economic and carbon objectives while accounting for battery degradation in replacement assessment; Fioriti et al. (2026) incorporated nonlinear asset degradation into multi-year off-grid microgrid planning with economic and environmental objectives. These studies differ in how aging enters the objective or assessment, but share a reliance on operating trajectories to evaluate degradation. Schedules with the same throughput can nevertheless differ in SOC residence and hourly cycling exposure.

Trajectory dependence is particularly relevant to representative-day planning, where an operating day is often required to finish at its initial SOC. Here, terminal-SOC closure denotes the correction used to meet that daily

boundary condition. In evolutionary optimization, such corrections restore feasibility before objective evaluation (Chootinan & Chen, 2006; Deb, 2000). Sanin-Villa et al. (2026) combined storage feasibility repair with degradation-aware scheduling. However, alternative feasible corrections can meet the same terminal SOC while producing different intermediate SOC and power profiles. An early correction affects the subsequent SOC path for longer than an equally sized late correction, and alternative timings can change cycling rates and their coincidence with temperature. The effect of these repair choices on modeled degradation has received comparatively limited attention, particularly when daily charging and discharging totals are separately preserved. Separately preserving daily charging and discharging totals defines the storage task in the paired comparison used here. It allows the effect of moving energy between hours to be examined without attributing a reduction in storage service to repair timing. In particular, a schedule that discharges less and relies more heavily on grid purchases represents a different service and cannot alone establish a timing effect.

This study jointly optimizes battery power, energy capacity and hourly dispatch for four seasonal representative days in a grid-connected microgrid. Its three-objective model has 98 decision variables: two battery ratings and 96 hourly dispatch genes. Both repair modes first apply the same terminal-SOC closure to each decoded candidate. The proposed refinement then exchanges equal amounts of charging or discharging energy between admissible hours. Each exchange is evaluated over the complete trajectory and accepted only when it satisfies the specified operating, task-preservation, degradation and operating-cost requirements.

The study contributes this task-preserving refinement and evaluates its effect through paired fixed-capacity trajectories, shared-candidate-pool selection and degradation-model sensitivity. For each candidate, the paired comparison isolates changes in timing between the two trajectories. The shared-pool comparison examines how alternative criteria select from the same feasible proposals, while sensitivity tests assess dependence on aging assumptions. To assess search performance, improved NSGA-II, standard NSGA-II, SPEA2 and MOEA/D are compared under a common evaluation budget. A separate equal-weight TOPSIS analysis summarizes the cost, carbon and degradation trade-offs among three representative dispatch strategies; it is distinct from the selection of each algorithm's representative solution.

2 System model and optimization formulation

2.1 Energy flows and operating constraints

The grid-connected microgrid comprises wind and photovoltaic generation, local demand, battery storage and a utility connection (Fig. 1). Wind and PV generation and requested demand are prescribed as hourly power profiles for each representative season; their capacities are not decision variables. Renewable generation first serves

demand. Surplus may charge the battery, be exported or be curtailed, whereas the battery and grid serve deficits. The model uses an aggregated energy balance rather than a network power-flow calculation:

$$P_{d,t}^{WT} + P_{d,t}^{PV} + P_{d,t}^{dis} + P_{d,t}^{buy} = P_{d,t}^{L} + P_{d,t}^{ch} + P_{d,t}^{sell} + P_{d,t}^{curt} \quad (1)$$

In Equation (1), PL is served demand, equal to requested demand L minus unserved power Pu; $0 \le Pu \le L$, and unserved energy incurs a penalty. With power in MW, nominal energy EB in MWh and $\Delta t = 1$ h, the battery SOC follows:

$$s_{d,t} = s_{d,t-1} + \frac{\eta_{ch} P_{d,t}^{ch} - \frac{P_{d,t}^{dis}}{\eta_{dis}}}{E_B} \Delta t \quad (2)$$

Both efficiencies are 0.95. Battery sizing is restricted to 18–45 MW, 50–115 MWh, and nominal duration EB/PB of 2.2–3.0 h. Grid import/export limits are 180/36 MW. Charging and discharging are mutually exclusive. Initial SOC is 0.55, with the following path and daily closure constraints:

$$s_{min} \le s_{d,t} \le s_{max}, \quad |s_{d,24} - s_{d,0}| \le \varepsilon_{SOC} \quad (3)$$

For requested demand L, the renewable surplus S and deficit H at each hour are defined from the prescribed wind and PV inputs:

$$S = max(P_{WT} + P_{PV} - L, 0), \quad H = max(L - P_{WT} - P_{PV}, 0) \quad (3a)$$

The battery can charge only from renewable surplus and discharge only to a local deficit. Its charging and discharging powers are bounded by rated power PB:

$$0 \le P_{ch} \le min(P_B, S), \quad 0 \le P_{dis} \le min(P_B, H) \quad (3b)$$

Grid imports and exports are bounded by their respective connection ratings:

$$0 \le P_{buy} \le P_{buy,max}, \quad 0 \le P_{sell} \le P_{sell,max} \quad (3c)$$

Under the surplus/deficit allocation, charging and discharging are mutually exclusive, as are grid imports and exports. These restrictions prohibit grid-to-battery charging and battery-to-grid export. The remaining renewable surplus after charging and export is curtailed; any remaining deficit after discharge and grid purchases is unserved demand. The displayed hourly wind, PV and demand profiles are direct case inputs; the optimization does not reconstruct them from wind speed or irradiance.

The four 24-hour seasonal wind, PV and demand profiles were obtained by applying K-means clustering to annual 8,760-hour records. The seasonal weights are set to 90, 92, 91 and 92 days, respectively. Each representative day is independently closed, with SOC bounds of 0.10–0.90 and $\varepsilon SOC = 10^{-5}$; chronological SOC continuity across

seasons is not imposed. The selected hourly inputs are listed in Additional file 1, Tables S12–S15. Battery-cabin temperature is prescribed separately, and heating/cooling auxiliary consumption is excluded.

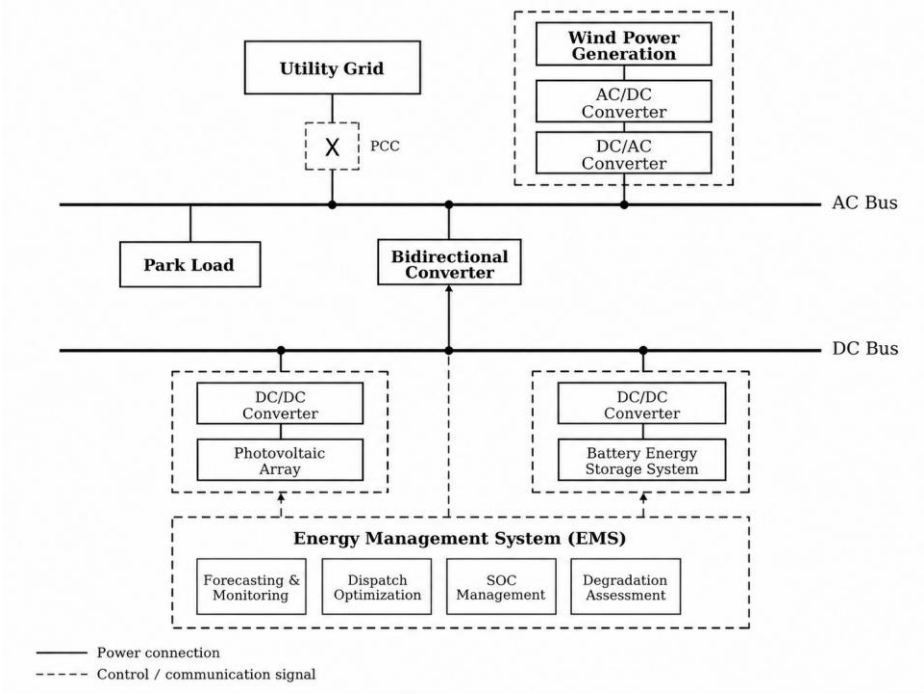


Fig. 1 Architecture of the grid-connected wind–photovoltaic–storage microgrid

2.2 First-year Arrhenius degradation

Calendar and cycling losses are accumulated separately. The normalized temperature factor uses activation energy Ea = 25,000 J mol^{-1}, gas constant R = 8.314 J mol^{-1} K^{-1}, and reference temperature Tref = 298.15 K:

$$\varphi_{d,t} = exp[-\frac{E_a}{R}(\frac{1}{T_{d,t}+273.15} - \frac{1}{T_{ref}})] \quad (4)$$

Internal charge-plus-discharge throughput defines the equivalent-full-cycle rate r, expressed in EFC h^{-1}:

$$r_{d,t} = \frac{\eta_{ch}P_{d,t}^{ch} + \frac{P_{d,t}^{dis}}{\eta_{dis}}}{2E_B} \quad (5)$$

The hourly cycling-loss and calendar-loss fractions are:

$$q_{d,t}^{cyc} = A_{cyc}{r_{d,t}}^{z}\varphi_{d,t}\,[1 + 0.18\,min(1.5, \frac{r_{d,t}}{0.030})]\,\Delta t \quad (6a)$$

$$q_{d,t}^{cal} = \frac{A_{cal}}{24}\varphi_{d,t}\,[1 + 0.75\,(\frac{max(s_{d,t-1} - 0.62, 0)}{0.33})^2]\,\Delta t \quad (6b)$$

Acyc = 1.2 × 10^{-5}, z = 0.65, and Acal = 2.5 × 10^{-6} day^{-1}. Calendar stress uses interval-start SOC. These effective coefficients and all remaining parameters are documented in Additional file 1, Tables S3–S5. The first-year percentage capacity loss is:

$$D_{annual} = 100 \sum_{d=1}^{4} w_d \sum_{t=1}^{24} (q_{d,t}^{cal} + q_{d,t}^{cyc}) \quad (7)$$

In the adopted model, the Arrhenius factor accounts for the effect of battery-cabin temperature on both calendar and cycling losses. Calendar loss also depends on the interval-start SOC: the SOC stress increases quadratically above the reference SOC of 0.62. Cycling loss depends on the hourly equivalent-full-cycle rate, which is determined by charging and discharging power, conversion efficiencies and rated battery energy. Consequently, schedules with identical daily charging and discharging totals can yield different modeled losses when their SOC residence, hourly power distribution or coincidence with temperature differs. Hourly calendar and cycling losses are summed using the seasonal day weights to obtain first-year capacity loss. The coefficients are effective case parameters, and cycle depth is not explicitly counted through rainflow analysis.

2.3 Planning objectives

The decision vector contains battery power, energy capacity, and 96 signed hourly genes. A deterministic decoder maps the genes to dispatch under source–load, SOC-reference, and price guidance. The planning problem minimizes:

$$min_{x \in \mathcal{F}} f(x) = [C_{annual}, G_{annual}, D_{annual}] \quad (8)$$

Annual cost comprises annualized battery and PCS investment, weighted daily operating cost and a residual terminal-SOC penalty:

$$C_{annual} = c_B \, ECRF_B + c_{PCS} \, PCRF_{PCS} + \sum w_d C_{d,op} + C_{term} \quad (8a)$$

Here E and P are rated battery energy (kWh) and PCS power (kW); cB and cPCS are their unit investment costs. The daily operating cost is

$$C_{d,op} = \sum (\pi_b P_b - \pi_s P_s + c_{PV} P_{PV} + c_W P_W + c_{om}(P_{ch} + P_{dis}) + c_c P_c + c_u P_u) \, \Delta t \quad (8b)$$

The sum is over the 24 hours of day d. Subscripts b and s denote grid purchase and sale; c and u denote curtailment and unserved demand. The terms comprise trading, PV and wind O&M, battery throughput O&M and the two penalties. Power is in kW, Δt = 1 h and prices and coefficients are in CNY/kWh. The terminal penalty is Cterm = λ∑d wd max(0, |SOCd,end − SOC0| − εSOC)/∑d wd, where λ = 8.0 × 10^7 CNY and εSOC = 10^{-5}.

$$CRF_j = i(1 + i)^{Nj} / [(1 + i)^{Nj} - 1] \quad (8c)$$

The capital recovery factor uses discount rate i = 0.08 and fixed annualization periods NB = 10 years for the battery and NPCS = 15 years for the PCS. These economic assumptions are independent of the modeled first-year capacity loss and are not degradation-derived lifetime estimates.

Annual carbon emissions include grid purchases, wind and PV generation, and the annualized embodied emissions of battery capacity:

$$G_{annual} = \sum w_d \sum(\gamma_{grid} P_{buy} + \gamma_{PV} P_{PV} + \gamma_W P_W)\,\Delta t + \gamma_B\, E / N_B \quad (8d)$$

Here γgrid, γPV and γW are emission intensities in $kgCO_2e/kWh$ of purchased electricity or generation, and γB is embodied emissions per installed kWh. Wind/PV coefficients in Additional file 1, Table S5 are converted from grams to kilograms. Exported electricity receives no avoided-emission credit. The battery embodied term uses the same assumed 10-year allocation period; no PCS embodied-emissions term is added. The first-year degradation objective is given by Equation (7), and all input coefficients are listed in Additional file 1, Table S5.

3 Degradation-aware trajectory refinement and search protocol

3.1 Common closure and task-preserving redistribution

Both repair modes start from the same decoded schedule and first apply common terminal-SOC closure. If terminal SOC is too low, existing discharge is removed in reverse time order, followed by adding feasible charging in forward order. If it is too high, charging is removed and feasible discharge added using the corresponding orders. Each correction is limited by the remaining imbalance, source–load and power availability, and the minimum future SOC margin; the trajectory is recomputed after each move. The degradation-aware stage is applied only after this closure converges.

Let superscript conv denote the common-closed schedule. The degradation-aware stage separately shifts charging or discharging between a donor hour a and a receiver hour b, preserving each daily energy total:

$$\sum_{t=1}^{24} P_{d,t}^{ch,new} = \sum_{t=1}^{24} P_{d,t}^{ch,conv}, \quad \sum_{t=1}^{24} P_{d,t}^{dis,new} = \sum_{t=1}^{24} P_{d,t}^{dis,conv} \quad (9)$$

For an operation m ∈ {ch, dis}, one candidate decreases donor power by δ and increases receiver power by the same amount; the other operation and all other hours remain unchanged:

$$P_{a,new} = P_a - \delta, \quad P_{b,new} = P_b + \delta \quad (9a)$$

The operation superscript m is omitted in Equation (9a) for readability. With equal one-hour intervals and fixed efficiencies, the separate charge/discharge totals, terminal SOC and EFC are preserved. Donors have positive power and receivers have spare capacity. The maximum trial power transfer is

$$\delta_{max} = min\{P_a, P_{cap,b} - P_b, \delta_{SOC}\}, \quad \delta \in \{\delta_{max}, 0.5\delta_{max}, 0.25\delta_{max}\} \quad (9b)$$

Receiver capacity Pcap,b is the minimum of rated power, the common-closed schedule's peak power for that operation and local renewable surplus for charging or local demand deficit for discharging. Let μ be the smallest SOC margin over the affected interval: to the upper limit if the transfer raises SOC there, or to the lower limit if

it lowers SOC. These limits are the tighter of the physical bounds and the common-closed trajectory extrema. The SOC-limited transfer is Eμ/(ηch Δt) for charging and Eμηdis/Δt for discharging, with E in kWh, Δt = 1 h and δ in kW.

For each admissible donor–receiver pair and trial amount, the complete SOC and power-balance trajectories are recomputed. Candidates must preserve daily grid purchases and unserved energy and keep trading, curtailment and unserved-energy cost no greater than the common-closed baseline, within numerical tolerance. Arrhenius calendar and cycling losses are evaluated over the complete day using its prescribed temperature profile. Relative to the current accepted trajectory, neither component may increase and their sum must decrease:

$$q_{cal,new} \leq q_{cal,k}, \quad q_{cyc,new} \leq q_{cyc,k}, \quad Q_{new} < Q_k \tag{9c}$$

Here qcal and qcyc are daily loss fractions and Q = 365(qcal + qcyc) is the repeated-day proxy used for ranking. Component comparisons use a 10^{-12} relative numerical tolerance; the required proxy decrease is greater than $\max(10^{-14}, 10^{-8}|Qk|)$. At each step, the valid candidate with minimum Q is selected and rechecked with the scalar trajectory model. The search stops when no qualifying improvement remains, a recheck fails, or eight exchanges have been accepted. The cost and service constraints are checked against the common-closed baseline; component losses are checked against the current accepted trajectory. Temperature influences modeled loss and electricity prices influence the cost check, without imposing a fixed temperature- or price-based hour ranking.

3.2 Controlled selection and degradation sensitivity

To examine selection under identical candidate opportunities, a separate shared-pool experiment starts from each run-specific, common-closed seasonal schedule. Battery power and energy are fixed. Each proposal is generated by moving equal amounts of charging energy or discharging energy between admissible hours; a proposal may contain up to eight exchanges. The complete SOC trajectory is recomputed, and source–load availability, SOC margins and the original peak-power limits are respected. A fixed-seed procedure generates up to 256 distinct proposals at the same battery rating, together with the unchanged common-closed schedule.

The same candidate pool is evaluated using two selection criteria. Both require preserved daily charge, discharge, grid purchase and unserved energy, together with nonincreasing trading and curtailment cost. The cost selector chooses the lowest operating cost, using squared battery power to break ties. The degradation-aware selector chooses the lowest modeled loss and also requires calendar and cycling loss not to exceed their common-closure values. Thus, their comparison includes the additional component-loss guards. The main iterative refinement uses a separate adaptive exchange sequence and is evaluated independently.

Seventeen cases test the influence of the degradation model by varying the rate exponent, activation energy, rate and SOC stress, calendar/cycling coefficients and temperature dependence. First, the nominal closed and refined trajectories are revalued at fixed capacity without changing dispatch. Second, the unchanged physical pool is rescored and the degradation-aware selection is repeated. The anchored linear case S04 also removes the additional rate-stress term. Cases and results are listed in Additional file 1, Tables S22 and S25.

The three common-capacity dispatch strategies are also assessed using hourly SOC, grid purchases and modeled loss. The same pool-based aging selection is applied separately to each strategy while preserving its own daily charging and discharging totals; service volumes may differ across strategies.

3.3 Improved NSGA-II search

The improved algorithm modifies how candidates are generated and retained relative to standard NSGA-II. Both begin with the paired common initial population. The improved method additionally evaluates 17 objective-oriented initial candidates and selects the initial population from the combined set. In each generation it produces offspring using differential evolution (DE/rand/1) and simulated binary crossover (SBX), followed by polynomial mutation. Approximately 52% of the regular offspring are assigned to the DE branch. In the SBX branch, crossover and mutation probabilities are adjusted using nondominated rank and normalized objective values.

Every fourth generation, structured local candidates are generated around selected nondominated solutions by perturbing battery ratings or a seasonal dispatch block. Parents and offspring are combined for environmental selection. Nondominated fronts are admitted in order; when the next front exceeds the remaining slots, the method retains objective extremes and then selects solutions separated in normalized objective space. By contrast, the standard NSGA-II uses SBX, polynomial mutation and nondominated sorting with crowding-based selection. The additional candidates are included in the search-evaluation budget. All algorithms use the same system model and default repair settings, so the trajectory refinement and the search modifications are assessed as distinct elements.

3.4 Benchmark and representative-solution selection

Improved NSGA-II is compared with standard NSGA-II (Deb et al., 2002), SPEA2 (Zitzler et al., 2001), and MOEA/D (Zhang & Li, 2007). Each uses population 96 and 24,000 search objective evaluations per run, including initialization, offspring and additional candidates. Twelve independent runs use paired seeds and common initial populations. Operator settings are given in Additional file 1, Tables S9–S10. Equal search-evaluation counts do not imply identical repair-internal computation.

A deterministic 120-point pilot, outside the search budget, establishes common normalization bounds for the indicators and representative-solution selection. IGD uses an empirical reference formed from the pooled

nondominated final fronts, sampled to at most 360 points. Normalized HV uses reference (1.2, 1.2, 1.2) and divisor 1.728. For each algorithm, the representative run is the run whose IGD is nearest its median across 12 runs. Within that run, a feasible solution minimizing the equally weighted normalized objective sum is selected. The reported rating is therefore an actual solution, not an average across runs.

The optimized, renewable-priority and TOU strategies are then compared at the selected common battery rating. Equal-weight TOPSIS uses annual cost, carbon emissions and modeled first-year loss as cost-type criteria (Hwang & Yoon, 1981). Each criterion is min–max scaled over the three strategies, and distances to the zero ideal and unit negative ideal give the closeness coefficient. This post hoc strategy ranking is separate from the representative-solution selection.

4 Results and discussion

4.1 Search performance and capacity–dispatch trade-offs

Table 1 compares the final approximation sets obtained by the four algorithms under the same search-evaluation budget. Across 12 independent runs, improved NSGA-II attains an IGD of 0.02840 ± 0.00168 and a normalized HV of 0.84665 ± 0.00444. Relative to standard NSGA-II, the mean IGD decreases by 66.55% and the mean HV increases by 16.37%. The improved algorithm also has the lowest mean IGD and highest mean HV among the four methods. Its mean search time is 671.84 s, compared with 692.91 s for standard NSGA-II. These results indicate a better approximation of the pooled empirical reference front under the stated evaluation budget.

Table 1. Search performance under a common evaluation budget.

Algorithm	IGD	Normalized HV	Time (s)
Improved NSGA-II	0.02840 ± 0.00168	0.84665 ± 0.00444	671.84 ± 41.24
Standard NSGA-II	0.08489 ± 0.01076	0.72758 ± 0.01036	692.91 ± 49.92
SPEA2	0.07687 ± 0.01118	0.72235 ± 0.01463	691.95 ± 34.71
MOEA/D	0.11597 ± 0.01861	0.65302 ± 0.02321	695.54 ± 46.12

Values are mean ± sample standard deviation for 12 independent runs; each algorithm uses 24,000 search objective evaluations per run.

Table 2 lists the selected feasible configuration and objectives for each algorithm. The improved-NSGA-II solution is used as the common rating in the following dispatch comparison.

Table 2. Selected capacity and three objectives for each algorithm.

Algorithm	Power MW	Capacity MWh	Annual cost 10^4 CNY	Annual carbon 10^4 kg	First-year loss (%)
Improved NSGA-II	40.49	114.97	5333.72	7023.88	0.86322
Standard NSGA-II	43.46	113.90	5440.56	6882.19	0.92691
SPEA2	39.40	114.77	5398.26	7037.60	0.85512
MOEA/D	39.76	114.98	5326.24	6916.15	0.92703

Each row is one feasible solution from its algorithm's representative run, not an average across runs. The selected runs are 11, 6, 7 and 3, respectively. Annual results are weighted sums of four seasonal typical days.

4.2 Seasonal dispatch at a common battery rating

Fig. 2 compares summer and winter dispatch for the three strategies at 40.4885 MW/114.9735 MWh. Renewable priority responds to current surplus or deficit; the TOU rule also uses price thresholds. The optimized schedule coordinates the daily profile with cost, emissions and modeled degradation. Positive stacks denote generation, discharge and purchases; negative stacks denote load, charging, exports and curtailment. Curves show net load and net grid exchange.

In summer, the optimized schedule leaves the battery uncharged during hours 3–5 and exports the renewable surplus, preserving SOC headroom for the later photovoltaic increase. In contrast, both rule-based schedules charge during these early hours; under renewable priority the battery reaches its upper SOC limit by hour 5. At hour 10, optimized dispatch uses part of the rising surplus to charge while retaining export, and at hour 11 its remaining headroom allows 25.1 MW of charging, compared with 0.5 MW under renewable priority. With the export limit binding, the corresponding curtailed power is 35.3 MW rather than 59.8 MW. The optimized schedule still reaches the upper SOC limit, so midday curtailment is not eliminated; the benefit in this case is the better timing of available headroom.

The later summer use of stored energy also illustrates how the schedule coordinates successive deficit periods. Renewable priority discharges more heavily at hour 17, while optimized dispatch allocates part of its discharge to hour 18, when the purchase tariff is higher. The TOU rule defers discharge at hour 17 and relies on grid purchases; optimized dispatch supplies part of that deficit from storage and continues discharging at hour 18. This allocation

balances discharge during the hour-17 deficit against the value of retaining energy for the higher-price period at hour 18.

In winter, the optimized schedule charges from early renewable surplus and discharges during the morning deficit. Unlike renewable priority, which reaches the lower SOC bound by hour 10, it retains part of its stored energy. At hour 12 it exports the available surplus; at hour 13 it charges again, then supplies the hour-15 deficit. At the higher-price hour 18, this retained energy permits 11.6 MW of discharge, whereas the renewable-priority battery is at its lower SOC bound. The TOU rule supplies the hour-18 deficit more fully, but does not discharge at hour 15. The optimized trajectory therefore combines support across these deficit periods with renewable export and subsequent charging, rather than applying a single immediate-surplus or price threshold rule.

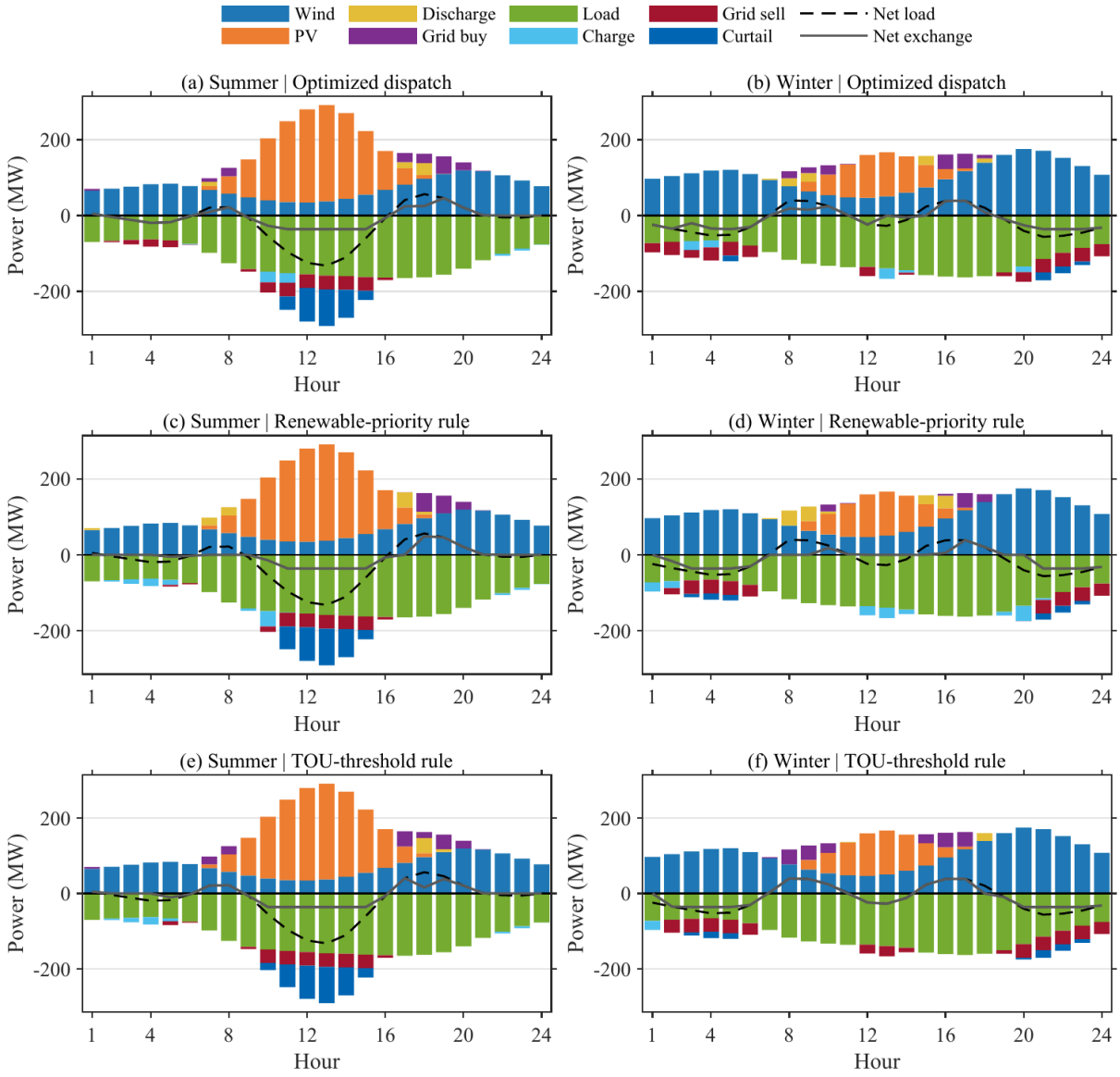


Fig. 2 Summer (left) and winter (right) energy balances at a common rating. Rows: optimized dispatch (a, b), renewable-priority rule (c, d), and TOU-threshold rule (e, f)

The annual accounting in Table 3 is consistent with these differences in energy allocation. Relative to renewable priority, optimized dispatch has higher purchase expenditure, but also greater export revenue and lower curtailment penalty; their combined effect, together with lower battery-throughput O&M, reduces annual cost. Its modeled loss is also lower, although annual battery discharge is smaller and grid purchases and emissions are higher. Relative to TOU, the optimized schedule reduces annual cost and emissions while delivering more battery discharge, with a higher modeled loss. These outcomes illustrate the cost–emission–degradation trade-off: the operational advantage is coordinated allocation across the day, while the direction of improvement depends on the criterion and storage-service volume.

Table 3. Annual strategy comparison at the representative battery rating.

Strategy	Cost 10^4 CNY	Carbon 10^4 kg	Loss %	Discharge MWh	Grid buy MWh
Optimized dispatch	5333.72	7023.88	0.86322	24207.05	33093.25
Renewable-priority rule	5957.58	5853.33	1.28767	38838.85	18461.44
TOU-threshold rule	5814.66	8040.86	0.48220	11494.80	45805.49

Representative improved-NSGA-II run 11 at 40.4885 MW/114.9735 MWh. Annual values use seasonal typical-day weights; storage-service volumes differ between strategies.

The equal-weight TOPSIS comparison summarizes the three objectives in Table 3. Optimized dispatch has the highest closeness coefficient, 0.631, followed by TOU at 0.448 and renewable priority at 0.414 (Table 4). Within this comparison, the result reflects the lowest cost together with intermediate carbon emissions and modeled degradation. The ranking applies to the stated equal weights and the three selected alternatives.

Table 4. Equal-weight TOPSIS ranking of the three representative dispatch strategies.

Strategy	Closeness coefficient	Rank
Optimized dispatch	0.631	1
TOU-threshold rule	0.448	2
Renewable-priority rule	0.414	3

Representative run 11; equal weights of 1/3 for cost, carbon and first-year loss. Min–max scaling and ideal points use only the three strategies in Table 3.

A separate shared-pool postprocessing comparison starts from each strategy's common terminal-SOC closure and preserves that strategy's own daily charging and discharging totals. The resulting first-year losses are 0.94152%, 1.27124% and 0.47715% for the optimized, renewable-priority and TOU strategies, respectively. These are postprocessed trajectories and differ from the representative strategy schedules evaluated in Table 3.

4.3 Paired repair effects and hourly mechanism

The paired repair experiment holds the decoded candidate, battery rating and daily charging and discharging energy fixed within each comparison. Table 5 shows that, across 12 run-specific candidates, conventional repair gives a modeled first-year loss of 0.95412 ± 0.04808%, while degradation-aware refinement gives 0.85223 ± 0.04816%. The mean of the 12 paired relative reductions is 10.70% ± 1.11%. For the representative candidate, loss falls from 0.97657% to 0.86322%, a reduction of 11.61%. These paired results isolate the effect of redistributing the prescribed storage task within the adopted model.

Table 5. First-year degradation under paired repair methods.

Degradation component	Conventional loss (%)	Degradation-aware loss (%)	Paired reduction (%)
Calendar loss	0.10318 ± 0.00083	0.09622 ± 0.00150	6.73 ± 2.05
Cycling loss	0.85094 ± 0.04844	0.75601 ± 0.04741	11.18 ± 1.11
Total loss	0.95412 ± 0.04808	0.85223 ± 0.04816	10.70 ± 1.11

Mean ± sample standard deviation across 12 paired candidates. Relative reductions are calculated per run before averaging; charge and discharge are matched within each pair.

For the representative candidate, calendar loss decreases from 0.10345% to 0.09698%, while cycling loss decreases from 0.87313% to 0.76625%. The cycling component accounts for approximately 94.3% of the total absolute reduction. The following trajectory comparison examines how these changes arise under the adopted model.

Fig. 3 compares the common-closed schedule and its degradation-aware refinement at the same battery rating. In summer, the refined SOC remains below the conventional trajectory during part of the early and middle day before both reach the upper SOC limit around midday. Its time-mean SOC decreases from 66.61% to 62.45%, and calculated residence above 80% SOC falls from 6.86 to 6.15 h. In winter, the refined trajectory also spends less time at elevated SOC during the morning and midday; mean SOC falls from 67.37% to 60.89%, and residence above 80% falls from 6.71 to 4.03 h. Residence above 80% SOC is calculated by linearly interpolating

SOC between successive hourly values. Both methods end at 55% SOC. The gray trajectory is the decoded schedule before terminal closure, whereas the paired comparison uses the two closed trajectories.

The power panels explain how the SOC changes are achieved: charging or discharging is shifted between admissible hours through equal-energy exchanges. In summer, both closed schedules retain 65.54 MWh of charging and 59.15 MWh of discharge; in winter, they retain 91.04 and 82.16 MWh, respectively. The comparison therefore holds daily battery service fixed while changing its timing. In the calendar-loss model, SOC above 0.62 increases the hourly stress factor; reducing portions of high-SOC residence can therefore lower cumulative calendar loss. Lower daily mean SOC alone does not determine the loss, which is evaluated from the complete hourly SOC and temperature profiles.

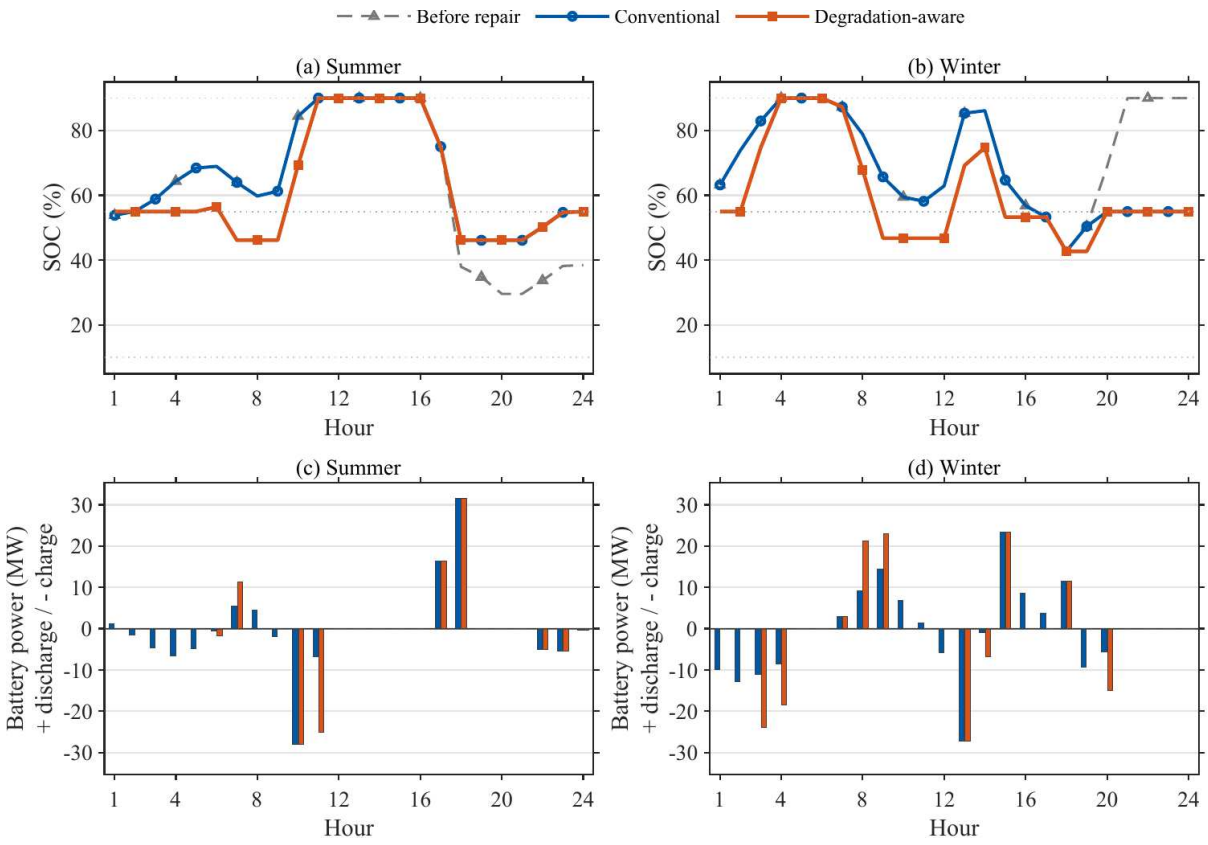


Fig. 3 Paired summer/winter interval-end SOC (a, b) and battery power (c, d). Positive power denotes discharge. Gray paths precede terminal closure; repaired trajectories share the 55% terminal target

Cycling loss is evaluated from the full trajectory using the hourly charge/discharge rate and prescribed battery-cabin temperature. The candidate exchanges alter power timing and its temperature coincidence even when throughput is unchanged. The refinement compares complete trajectory losses, accepts only feasible exchanges that lower total modeled loss without increasing either component, and requires trading plus curtailment cost not to increase. Electricity prices enter this cost check; temperature enters the aging calculation. Thus, the result does

not imply that every accepted exchange moves activity to a cooler or lower-price hour. For representative run 11, the uniform-25 °C cycling reduction is 0.11644 percentage points, compared with 0.10688 percentage points under the original temperature profile; the temperature-interaction residual is −0.00956 percentage points.

4.4 Selection with identical candidate opportunities

In each of the 12 runs and four seasons, the pool contains the unchanged common closure and 256 distinct proposals. Both selectors evaluate the same 257 physical trajectories. Relative to common closure, degradation-aware selection reduces modeled loss by 3.21% ± 0.53%, while cost selection increases it by 1.06% ± 0.89%. Charge, discharge, purchases and EFC are preserved; the degradation-aware selector also imposes component-loss guards. This controlled comparison is separate from the 10.70% mean reduction obtained by the main iterative refinement across the 12 paired candidates.

4.5 Rate dependence and interpretation of the degradation mechanism

The cycling term is rate dependent: at equal temperature and saturated rate stress, 0.10 EFC in one hour gives a cycling factor 21.54% smaller than the same throughput at 0.05 EFC h^{-1} over two hours. This is a property of the adopted model, not a general battery-aging rule.

Fig. 4 shows mean fixed-trajectory reductions of 10.70% ± 1.11% at baseline, 16.19% ± 1.54% at z = 0.50 and 5.25% ± 0.69% at z = 0.80. The anchored linear case S04, reported in Table S25 rather than plotted, gives 0.39% ± 0.28% on average, with two individual increases. S04 changes both the rate exponent and additional rate stress, illustrating the dependence of the result on the assumed cycling response.

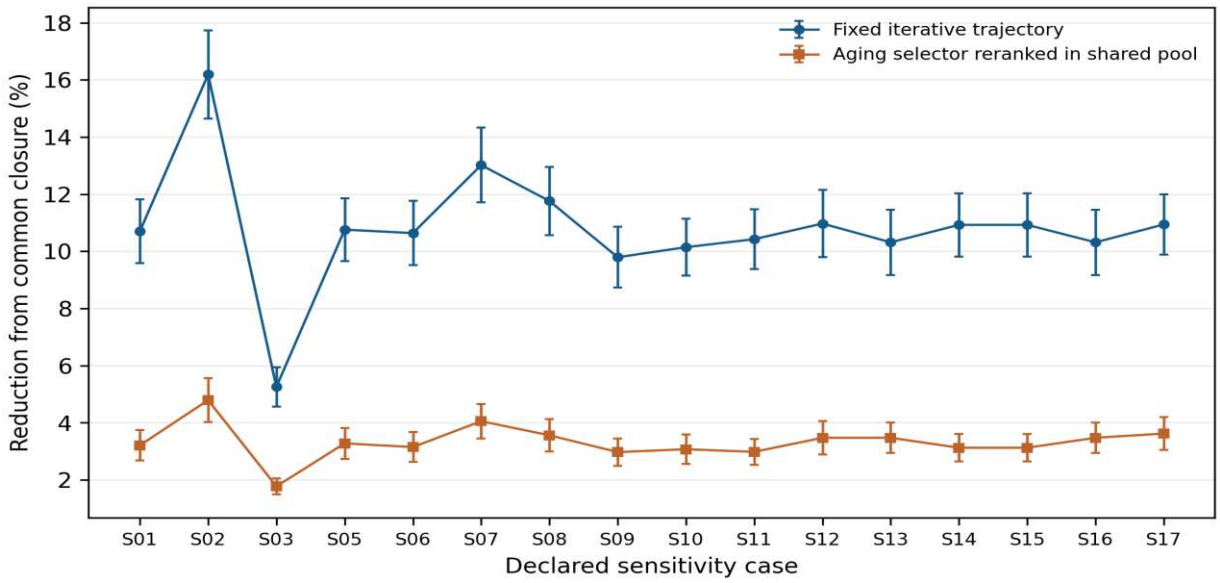


Fig. 4 Modeled loss reduction for fixed iterative trajectories and reranked shared-pool selection across 16 discrete cases. Lines are visual guides, not interpolation; error bars are sample standard deviations across 12 candidates. S04 is reported in Additional file 1, Table S25

Across all 17 settings, reranking the shared pool reduces modeled loss by 0.91–4.79% on average. The selector includes a nonincrease acceptance rule; the aging coefficients are effective case values.

5 Conclusions

This study combines capacity–dispatch optimization with a task-preserving, degradation-aware refinement of feasible battery schedules. Across 12 paired candidates, the refinement reduces modeled first-year capacity loss by 10.70% on average while preserving daily charging and discharging totals. At the representative rating, optimized dispatch coordinates renewable charging, discharge and grid exchange, achieving the highest equal-weight TOPSIS closeness among the three compared strategies. The common-pool experiment further demonstrates a 3.21% mean modeled-loss reduction under degradation-aware selection. Sensitivity analysis shows that the magnitude of the benefit depends on the adopted cycling response. Under the stated case assumptions, task-preserving temporal redistribution can reduce modeled battery degradation while maintaining the specified storage task and operating-cost constraints.

List of abbreviations

DE: differential evolution; EFC: equivalent full cycles; HV: hypervolume; IGD: inverted generational distance; MOEA/D: multiobjective evolutionary algorithm based on decomposition; NSGA-II: nondominated sorting genetic algorithm II; PCS: power conversion system; PV: photovoltaic; SBX: simulated binary crossover; SOC: state of charge; SPEA2: strength Pareto evolutionary algorithm 2; TOPSIS: technique for order preference by similarity to ideal solution; TOU: time of use.

Declarations

Competing interests

The authors declare no competing interests.

Funding

This work was supported by the Shandong Provincial Key Research and Development Program (Major Scientific and Technological Innovation Project), project “Research and Demonstration of Flexible Intelligent Grid Equipment” (Grant No. 2024CXGC010308).

Ethics approval

Not applicable. This study does not involve human participants, human data, animal experiments, or materials requiring ethical approval.

Consent to participate

Not applicable.

Consent for publication

Not applicable.

Authors' contributions

RW: conceptualization, methodology and writing—original draft. JW: software, formal analysis and data curation. XY: validation and visualization. WL: investigation and writing—review. ZQ: data processing and writing—review. JCW: supervision, project administration, and writing—review and editing. All authors read and approved the final manuscript. Author initials: RW, Ranran Wang; JW, Jiayu Wang; XY, Xinyu Yu; WL, Wenqiao Li; ZQ, Zeyu Qiu; JCW, Jiancheng Wang.

Availability of data and materials

The four seasonal hourly input profiles, principal model and search parameters, and sensitivity cases and results are provided in Additional file 1. The data that support the findings of this study are available from the corresponding author upon reasonable request.

Code availability

The code used in this study is available from the corresponding author upon reasonable request.

Additional files

Additional file 1 (PDF): Seasonal hourly inputs, model and search parameters, and degradation sensitivity cases and results for the 12-run study.

References

Agha Kassab, F., Celik, B., Locment, F., Sechilariu, M., Liaquat, S., & Hansen, T. M. (2025). Microgrid sizing with EV flexibility: Cascaded MILP and embedded APSO-MILP approaches. *Applied Energy, 396*, 126273. https://doi.org/10.1016/j.apenergy.2025.126273

Altimania, M. R. M., Basem, A., Saydullaev, B., Atamuratova, Z., Madaminov, B., Umarov, A., Benti, N. E., & Chaka, M. D. (2026). Adaptive multi-objective optimization of microgrid energy management using deep reinforcement learning considering battery degradation and renewable uncertainty. *Scientific Reports, 16*, 14296. https://doi.org/10.1038/s41598-026-44179-z

Amini, M., Khorsandi, A., Vahidi, B., Hosseinian, S. H., & Malakmahmoudi, A. (2021). Optimal sizing of battery energy storage in a microgrid considering capacity degradation and replacement year. *Electric Power Systems Research, 195*, 107170. https://doi.org/10.1016/j.epsr.2021.107170

Amini, M., Sanjareh, M. B., Nazari, M. H., Gharehpetian, G. B., & Hosseinian, S. H. (2024). A novel model for battery optimal sizing in microgrid planning considering battery capacity degradation process and thermal impact. *IEEE Transactions on Sustainable Energy, 15*(3), 1435–1449. https://doi.org/10.1109/TSTE.2024.3349391

Cardoso, G., Brouhard, T., DeForest, N., Wang, D., Heleno, M., & Kotzur, L. (2018). Battery aging in multi-energy microgrid design using mixed integer linear programming. *Applied Energy, 231*, 1059–1069. https://doi.org/10.1016/j.apenergy.2018.09.185

Chen, L., Gao, L., Xing, S., Chen, Z., & Wang, W. (2024). Zero-carbon microgrid: Real-world cases, trends, challenges, and future research prospects. *Renewable and Sustainable Energy Reviews, 203*, 114720. https://doi.org/10.1016/j.rser.2024.114720

Chootinan, P., & Chen, A. (2006). Constraint handling in genetic algorithms using a gradient-based repair method. *Computers & Operations Research, 33*(8), 2263–2281. https://doi.org/10.1016/j.cor.2005.02.002

Dai, X., & Batool, K. (2024). Optimizing multi-objective design, planning, and operation for sustainable energy sharing districts considering electrochemical battery longevity. *Renewable Energy, 229*, 120705. https://doi.org/10.1016/j.renene.2024.120705

Deb, K. (2000). An efficient constraint handling method for genetic algorithms. *Computer Methods in Applied Mechanics and Engineering, 186*(2–4), 311–338. https://doi.org/10.1016/S0045-7825(99)00389-8

Deb, K., Pratap, A., Agarwal, S., & Meyarivan, T. (2002). A fast and elitist multiobjective genetic algorithm: NSGA-II. *IEEE Transactions on Evolutionary Computation, 6*(2), 182–197. https://doi.org/10.1109/4235.996017

Dong, H., Fu, Y., Jia, Q., Zhang, T., & Meng, D. (2023). Low carbon optimization of integrated energy microgrid based on life cycle analysis method and multi time scale energy storage. *Renewable Energy, 206*, 60–71. https://doi.org/10.1016/j.renene.2023.02.034

Fallahifar, R., & Kalantar, M. (2023). Optimal planning of lithium ion battery energy storage for microgrid applications: Considering capacity degradation. *Journal of Energy Storage, 57*, 106103. https://doi.org/10.1016/j.est.2022.106103

Fioriti, D., Petrelli, M., Berizzi, A., & Poli, D. (2026). Microgrid planning by stochastic multi-objective multi-year optimization with capacity expansion and non-linear asset degradation. *Sustainability, 18*(8), 3785. https://doi.org/10.3390/su18083785

Gasper, P., Saxon, A., Shi, Y., Endler, E., Smith, K., & Thakkar, F. M. (2023). Degradation and modeling of large-format commercial lithium-ion cells as a function of chemistry, design, and aging conditions. *Journal of Energy Storage, 73*, 109042. https://doi.org/10.1016/j.est.2023.109042

Gharibvand, H., Gharehpetian, G. B., & Anvari-Moghaddam, A. (2024). A survey on microgrid flexibility resources, evaluation metrics and energy storage effects. *Renewable and Sustainable Energy Reviews, 201*, 114632. https://doi.org/10.1016/j.rser.2024.114632

Hwang, C.-L., & Yoon, K. (1981). *Multiple attribute decision making: Methods and applications.* Springer. https://doi.org/10.1007/978-3-642-48318-9

Jiménez-Vargas, I., Rey, J. M., & Osma-Pinto, G. (2023). Sizing of hybrid microgrids considering life cycle assessment. *Renewable Energy, 202*, 554–565. https://doi.org/10.1016/j.renene.2022.11.103

Jin, L., Kazemi, M., Comodi, G., & Papadimitriou, C. (2024). Assessing battery degradation as a key performance indicator for multi-objective optimization of multi-carrier energy systems. *Applied Energy, 361*, 122925. https://doi.org/10.1016/j.apenergy.2024.122925

Kassab, F. A., Celik, B., Locment, F., Sechilariu, M., Liaquat, S., & Hansen, T. M. (2024). Optimal sizing and energy management of a microgrid: A joint MILP approach for minimization of energy cost and carbon emission. *Renewable Energy, 224*, 120186. https://doi.org/10.1016/j.renene.2024.120186

Li, L.-L., Ji, B.-X., Li, Z.-T., Lim, M. K., Sethanan, K., & Tseng, M.-L. (2025). Microgrid energy management system with degradation cost and carbon trading mechanism: A multi-objective artificial hummingbird algorithm. *Applied Energy, 378*, 124853. https://doi.org/10.1016/j.apenergy.2024.124853

Mehmood, K. K., Khan, S. U., Lee, S. J., Haider, Z. M., Rafique, M. K., & Kim, C. H. (2017). Optimal sizing and allocation of battery energy storage systems with wind and solar power DGs in a distribution network for voltage regulation considering the lifespan of batteries. *IET Renewable Power Generation, 11*(10), 1305–1315. https://doi.org/10.1049/iet-rpg.2016.0938

Pinciroli, L., Baraldi, P., Compare, M., & Zio, E. (2023). Optimal operation and maintenance of energy storage systems in grid-connected microgrids by deep reinforcement learning. *Applied Energy, 352*, 121947. https://doi.org/10.1016/j.apenergy.2023.121947

Safavi, V., Mohammadi Vaniar, A., Bazmohammadi, N., Vasquez, J. C., Keysan, O., & Guerrero, J. M. (2025). A battery degradation-aware energy management system for agricultural microgrids. *Journal of Energy Storage, 108*, 115059. https://doi.org/10.1016/j.est.2024.115059

Sanin-Villa, D., Leyton-Valencia, K. A., & Grisales-Noreña, L. F. (2026). Multi-operator differential evolution for coordinated active and reactive battery scheduling in active distribution networks. *Sci, 8*(8), 212. https://doi.org/10.3390/sci8080212

Schmalstieg, J., Käbitz, S., Ecker, M., & Sauer, D. U. (2014). A holistic aging model for Li(NiMnCo)O2 based 18650 lithium-ion batteries. *Journal of Power Sources, 257*, 325–334. https://doi.org/10.1016/j.jpowsour.2014.02.012

Seger, P. V. H., Rigo-Mariani, R., Thivel, P. X., & Riu, D. (2023). A storage degradation model of Li-ion batteries to integrate ageing effects in the optimal management and design of an isolated microgrid. *Applied Energy, 333*, 120584. https://doi.org/10.1016/j.apenergy.2022.120584

Superchi, F., Moustakis, A., Pechlivanoglou, G., & Bianchini, A. (2025). On the importance of degradation modeling for the robust design of hybrid energy systems including renewables and storage. *Applied Energy, 377*, 124645. https://doi.org/10.1016/j.apenergy.2024.124645

Wang, Z., Wang, T., Niu, Q., Wu, J., Li, M., & Zhu, S. (2024). Research on multiobjective capacity configuration optimization of grid-connected wind-solar-storage microgrid system based on improved BWO algorithm. *Energy Science & Engineering, 12*(6), 2365–2384. https://doi.org/10.1002/ese3.1727

Xie, P., Jia, Y., Lyu, C., Wang, H., Shi, M., & Chen, H. (2022). Optimal sizing of renewables and battery systems for hybrid AC/DC microgrids based on variability management. *Applied Energy, 321*, 119250. https://doi.org/10.1016/j.apenergy.2022.119250

Zhang, Q., & Li, H. (2007). MOEA/D: A multiobjective evolutionary algorithm based on decomposition. *IEEE Transactions on Evolutionary Computation, 11*(6), 712–731. https://doi.org/10.1109/TEVC.2007.892759

Zhao, M., He, Y., Tian, Y., Sun, K., Jiao, L., & Wang, H. (2024). Capacity optimization of wind-solar-storage multi-power microgrid based on two-layer model and an improved snake optimization algorithm. *Electronics, 13*(21), 4315. https://doi.org/10.3390/electronics13214315

Zhou, Y. (2024). Renewable-storage sizing approaches for centralized and distributed renewable energy—a state-of-the-art review. *Journal of Energy Storage, 100*, 113688. https://doi.org/10.1016/j.est.2024.113688

Zitzler, E., Laumanns, M., & Thiele, L. (2001). *SPEA2: Improving the strength Pareto evolutionary algorithm (TIK Report No. 103).* ETH Zurich. https://doi.org/10.3929/ethz-a-004284029

Supplementary Files

This is a list of supplementary files associated with this preprint. Click to download.

- Additionalfile1updated.pdf